Carbohydrate Polymers 234 (2020) 115901

Contents lists available at ScienceDirect

Carbohydrate Polymers

journal homepage: www.elsevier.com/locate/carbpol

Clickable modular polysaccharide nanoparticles for selective cell-targeting

Kevin Peuler, Nathan Dimmitt, Chien-Chi Lin*

Department of Biomedical Engineering, Purdue School of Engineering & Technology, Indiana University-Purdue University Indianapolis, Indianapolis, IN 46202, USA

ARTICLE INFO

Keywords:
Nanoparticles
Heparin
Dextran
Norbornene-tetrazine reaction
Cell targeting

ABSTRACT

A therapeutic nanocarrier capable of cell targeting has the potential to reduce off-target effects of otherwise effective drugs. Nanoparticle surface modification can be tailored for specific cells, however multistep surface modification can prove slow and difficult for a variety of cell types. Here, we designed drug carrying polysaccharide based nanoparticles with a layered structure for clickable surface modification. The center of nanoparticle was composed of cationic macromer (e.g., poly-L-lysine) and anionic polysaccharide (e.g., heparin). Furthermore, a 'clickable' polysaccharide was installed on the surface of the nanoparticles to permit a wide range of bioconjugation via norbornene-tetrazine click chemistry. The utilities of these layered nanoparticles were demonstrated via enhanced protein sequestration, selective cell targeting (via PEGylation or altering polysaccharide coating), as well as loading and release of chemotherapeutic. The drug-loaded nanocarriers proved cytotoxic to J774A.1 monocytes and MOLM-14 leukemia cells.

1. Introduction

Nanoparticles have been widely used in a variety of biomedical applications. Depending on the intended applications and desired properties, nanoparticles can be fabricated with organic materials (e.g., polymers, liposomes, proteins) and/or inorganic elements (e.g., iron oxide, silica, gold). Polymeric nanoparticles are especially advantageous for drug delivery and cell/tissue targeting applications owing to the diverse arrays of natural and synthetic polymers available for biomedical applications. For example, Doxil®, a PEGylated liposomal doxorubicin formulation, was the first US Food and Drug Administration (FDA)-approved nanomedicine for cancer therapy (Tran, DeGiovanni, Piel, & Rai, 2017). While only a few dozens of nanomedicines have been approved by the FDA for clinical use (Bobo, Robinson, Islam, Thurecht, & Corrie, 2016), more than one hundred nanoparticular formulations are currently at different stages of clinical trials (Data available in Clinicaltrials.Gov).

Among the various routes to produce functional nanoparticles, electrostatic complexation is attractive for its simplicity in synthesis and diversity in materials selection. For example, positively charged polyethyleneimine (PEI) can complex with negatively charged DNA to form polyplexes for non-viral gene delivery (Zhang et al., 2018). On the other hand, conjugating PEG (i.e., PEGylation) on the surface of nanoparticles has several benefits, including extension of plasma circulation time, improvement of Enhanced Permeability and Retention (EPR) effect of nanoparticles for accumulation at the tumor site, and enhancing diffusion in mucus (Huckaby & Lai, 2018; Suk, Xu, Kim, Hanes, & Ensign, 2016). Polyelectrostatic complexes can be formed by simply mixing or vortexing positively and negatively charged polymers. For example, Chen et al. utilized simple stirring to fabricate nanoparticles composed of anionic heparin (Hep) and cationic poly-L-lysine (PLL) (Chen, Li, Liu, Ma, & Yan, 2016). However, this method can create nanocomplexes with high polydispersity index (PDI) that may not be ideal for translational applications (Danaei et al., 2018). Alternatively, ultrasonication can be employed to produce nanocomplexes with narrower size distribution and robust repeatability. Liu et al. used this approach to improve the fabrication of Hep/PLL nanoparticles (Liu et al., 2017). While ultrasonication may rapidly degrades fragile molecules (e.g., proteins or RNAs) (Phua, Nair, & Leong, 2014), this approach may be appropriate for rapidly generating synthetic drug loaded nanoparticles for drug delivery applications.

PEGylation has been used on many FDA-approved therapeutics, such as PEGylated interferon (Dumitrescu, Constantinescu, & Tanasescu, 2018). On the other hand, modifying nanoparticle surface with receptor-targeting ligands are essential in targeted delivery of nanoparticles to the desired site of action. For example, Okamoto et al. modified siRNA loaded lipid nanoparticles with antibodies for targeting breast cancer cells, which over-express heparin-binding epidermal growth factor (EGF) (Okamoto et al., 2018). Peng et al. modified heparin-cisplatin based nanoparticles with single-chain antibodies to recognize EGF receptor to successfully target and reduce lung cancer tumor volume (Peng et al., 2011). Labeling nanoparticle surface with a

* Corresponding author.
E-mail address: lincc@iupui.edu (C.-C. Lin).

https://doi.org/10.1016/j.carbpol.2020.115901
Received 18 November 2019; Received in revised form 3 January 2020; Accepted 20 January 2020
Available online 25 January 2020
0144-8617/ © 2020 Elsevier Ltd. All rights reserved.

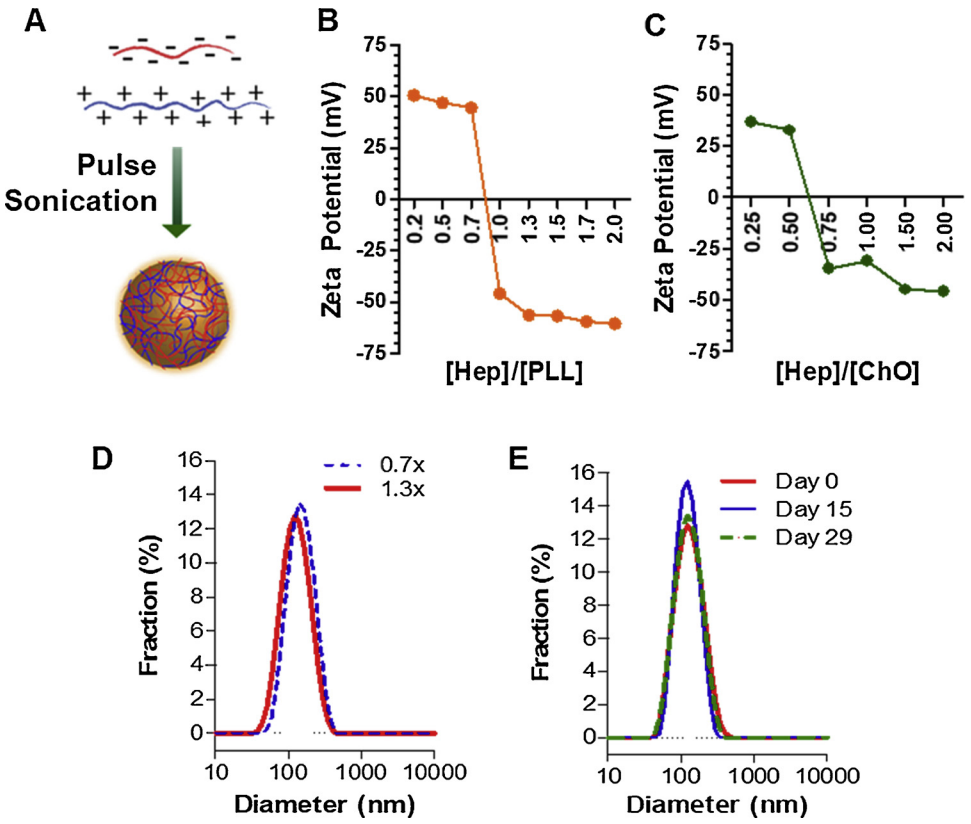

Fig. 1. (A) Schematic of ultrasonication-induced nanoparticle synthesis. (B) Zeta potential of NPs formed with varying [Hep]/[PLL] weight ratios. [PLL] = 0.25 mg/mL. (C) Zeta potential of NPs formed with varying [Hep]/[ChO] wright ratios. [ChO] = 0.25 mg/mL. (D) Size distribution of [Hep]/[PLL] NPs with weight ratios of 0.7x and 1.3 × . (E) Size distribution of [Hep]/[PLL] NPs (1.3x) at days 0, 15, and 29.

Table 1
Characterization of polysaccharide NPs with varying weight ratios of polyanion (Hep) and different polycation (A: PLL; B: ChO). [PLL] and [ChO] were fixed at 0.25 mg/mL.

A. [Hep]/[PLL]	Size (nm)	PDI
0.2	152.1 ± 2.6	0.172 ± 0.022
0.5	127.0 ± 1.3	0.208 ± 0.023
0.7	129.5 ± 7.4	0.166 ± 0.007
1.0	114.6 ± 4.2	0.176 ± 0.016
1.3	126.0 ± 6.5	0.199 ± 0.012
1.5	123.8 ± 5.8	0.220 ± 0.026
1.7	119.8 ± 4.5	0.174 ± 0.004
2.0	118.9 ± 0.4	0.173 ± 0.012
B. [Hep]/[ChO]	**Size (nm)**	**PDI**
0.25	323.5 ± 8.3	0.210 ± 0.023
0.50	261.4 ± 14.0	0.174 ± 0.016
0.75	283.2 ± 14.0	0.239 ± 0.021
1.00	258.7 ± 20.7	0.267 ± 0.024
1.50	262.9 ± 14.2	0.176 ± 0.013
2.00	249.8 ± 3.9	0.187 ± 0.006

'self-peptide' can also provide a camouflage against recognition by macrophages (Rodriguez et al., 2013). Various conjugation chemistries have been used to achieve robust functionalization of nanoparticle surface. For example, Tian et al. utilized carbodiimide chemistry to functionalize surface of heparin-quercetin based nanoparticles with LyP-1 peptide to target p32-overexpressing breast cancer cells (Tian et al., 2018). Surface modification of nanoparticles can also be achieved by 'Click Chemistry'. For instance, Han et al. utilized tetrazine-norbornene click reaction to label quantum dots with antibodies for in vivo single cell labeling (Han et al., 2010).

In this contribution, we report a modular approach for ultrasonication-based synthesis of layered nanoparticles composed of anionic Hep and cationic PLL at the center and additional polysaccharide was layered on the surface. The feed ratio of the core macromers (e.g., Hep and PLL) was adjusted to afford tunable surface charge. A second ultrasonication step was added to complex an additional layer of polysaccharide with an opposite charge. The modularity of the layered nanoparticles was demonstrated using anionic Hep, dextran sulfate (DS), as well as cationic PLL and chitosan oligosaccharide (ChO). Dynamic light scattering (DLS) was used to characterize surface charge and size distribution of the nanoparticles. The incorporation of Hep on nanoparticle surface was verified by dimethylmethylene blue (DMMB) assay. To afford modular labeling of nanoparticle surface (e.g., PEGylation or conjugation of other functional motif), Hep was modified with tetrazine or methyltetrazine (i.e., Hep-Tz or Hep-mTz). (methyl)tetrazine motif is a click chemistry handle that readily reacts with a norbornene-modified molecule. J774A.1, a monocyte/macrophage cell line was used to test the cytocompatibility and intracellular uptake of the nanoparticles formed by Hep/PLL and DS/PLL. Finally, the ability of these nanoparticles to serve as drug delivery carriers was evaluated with cytarabine, a standard chemotherapeutic agent used in treating acute myeloid leukemia.

2. Materials & methods

2.1. Materials

Poly-L-lysine hydrobromide (PLL, 120 kDa) was purchased from Polysciences Inc. Heparin sodium (Hep, 16.3 kDa) and chitosan oligosaccharide (ChO) were purchased from Celsus Laboratories and TCI America, respectively. Norbornene-2-carboxylic acid and diethyl ether were purchased from Sigma-Aldrich. Eight-arm PEG-OH (20 kDa) was purchased from JenKem Technology, USA. Derivatives of tetrazine were purchased from Click Chemistry Tools. Lipopolysaccharide (LPS) was purchased from Cell Signaling Technology. Saponin was purchased from Chem-Impex International Inc. 4′,6-Diamidino-2-phenylindole, dihydrochloride (DAPI) was purchased from Anaspec Inc. Sulfo-Cy5-

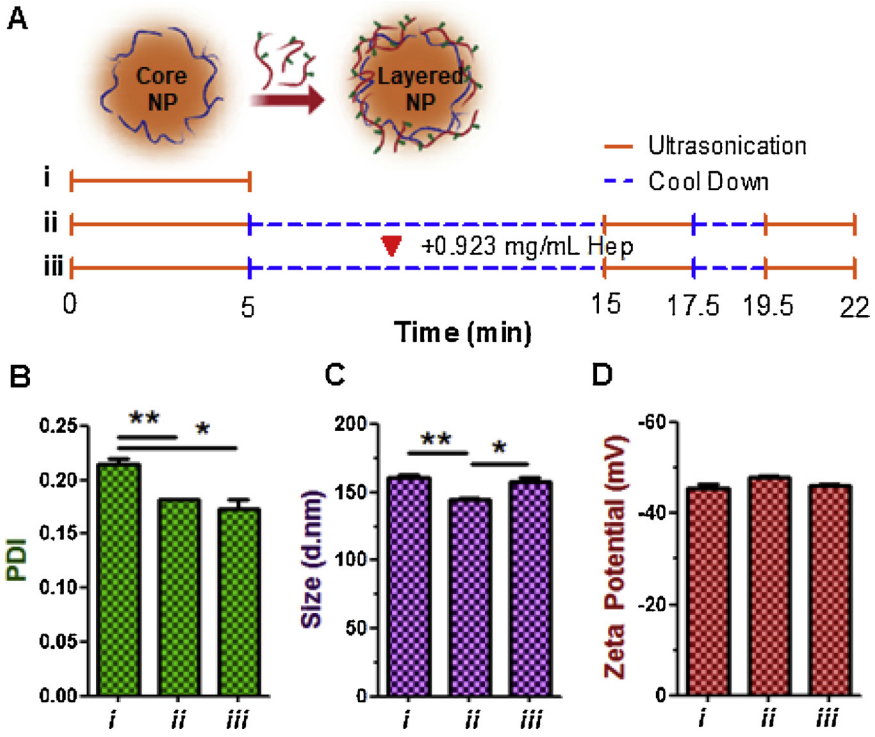

Fig. 2. (A) Schematic of layered NP fabrication. Starting materials in methods i & ii: 2 mg/mL Hep, 1.538 mg/mL PLL. Starting materials in method iii: 1.077 mg/mL Hep, 1.538 mg/mL PLL. Additional Hep (0.923 mg/mL) was added during the first cool-down period. (B–D) DLS characterization of NPs, including (B) PDI, (C) averaged size, and (D) Zeta potential. Single and double asterisks represent $p < 0.05$ and $p < 0.001$, respectively.

Table 2
DLS Measurements of layered nanoparticles (0.25 mg/mL PLL at the core).

Shell Polysaccharide	Zeta Potential (mV)	Size (nm)	PDI
Hep	−50.6 ± 0.6	123.2 ± 5.2	0.149 ± 0.011
DS	−50.2 ± 1.2	130.6 ± 2.0	0.144 ± 0.003
Hep-Tz	−46.8 ± 1.1	133.4 ± 3.2	0.136 ± 0.006
Hep-mTz	−42.6 ± 2.5	137.6 ± 2.1	0.126 ± 0.004

tetrazine was purchased from Santa Cruz Biotechnology. Lysozyme (purified, salt free) was obtained from Worthington Biochemical Corporation. All other chemicals were purchased from Fisher Scientific.

2.2. Macromer modification and synthesis

mTz/Tz modified heparins were synthesized via standard carbodiimide chemistry using 1-ethyl-3-(-3-dimethylaminopropyl) carbodiimide hydrochloride (EDC) and N-hydroxysuccinimide (NHS) as coupling reagents. Modified heparin was purified via dialysis (3500 Da MWCO) at room temperature for 48 h in ddH_2O and the resulting material was lyophilized. Substitution was determined via measuring mTz/Tz absorbance at 523 nm using a microplate reader (Synergy HT, BioTek). 5(6)-Carboxyflourescene modified PLL was also synthesized via the same carbodiimide crosslinker chemistry in ddH_2O. The product was purified by dialysis (6 − 8 kDa MWCO) at room temperature for two days in ddH_2O and then lyophilized. Photoinitiator Lithium Phenyl-2,4,6-trimethylbenzoylphosphinate (LAP) was synthesized according to previously reported method (Fairbanks, Schwartz, Bowman, & Anseth, 2009). Methyl-PEG-NB, linear PEG-diNB (6 kDa), and 8-arm PEG-NB (20 kDa) were synthesized as reported previously (Fairbanks, Schwartz, Bowman et al., 2009; Fairbanks, Schwartz, Halevi et al., 2009). ^{1}H NMR (Bruker Advance 500) was used to determine the degree of NB functionalization. Linear Cy5-PEG-NB was synthesized by mixing PEG-diNB with Cy5-Tz for 1 h. A NB/Tz ratio of 20 was used to ensure conjugation of Cy5-Tz to PEG-diNB.

2.3. Nanoparticle preparation & characterization

PLL and heparin were dissolved in filtered double distilled water ($fddH_2O$, pH 7.1) and sonicated in an ice bath using a Bronson Digital Sonifier (19.95 ± 0.10 kHz, 10 % amplitude) for an initial five minutes. For pulse sonication, a 10 min cool down period was added after the initial 5 min sonication, followed by an additional 2.5 min sonication, 2 min cool down, and 2.5 min sonication. The resulting solution was analyzed by dynamic light scanning (DLS) with Malvern Zetasizer Nano ZS90. For layered NP fabrication, the core NPs were prepared using PLL (0.25 mg/mL) and heparin (0.175 mg/mL) at a Hep/PLL ratio of 0.7. The surface polysaccharide was added during the first cooling step. The final weight ratio of polyanion/polycation was 1.3 × . Dimethyl methylene blue (DMMB) reagent was prepared by adding 16 mg DMMB zinc chloride into 1 L of double distilled water containing 3.04 g glycine, 1.6 g sodium chloride, and 95 mL of 0.1 M acetic acid (Farndale, Buttle, & Barrett, 1986). Heparin content in the solution was quantified by measuring DMMB absorbance at 523 nm. To quantify Tz-NB reaction, methyl-PEG-NB and mTz-heparin were separately dissolved in deuterium oxide. The solutions were mixed together at a 3:2 mTz:NB ratio and added to an NMR tube. The reaction was characterized by ^{1}H NMR (Bruker Advance 500).

2.4. Characterization of clickable NPs and NP-laden hydrogels

PEGylation of NPs was demonstrated by clicking Cy5-PEG-NB to Tz-heparin coated NPs. Tz:NB ratio was fixed at 1 and the components were mixed for 24 h, followed by separating the unreacted Cy5-PEG-NB via centrifugation (25 min at 14,000 rpm). The NP pellet was re-suspended in ddH_2O and the process was repeated twice. Cy5-PEG-NPs (7.3 wt%) were encapsulated in hydrogels formed by PEG8NB (3 wt%), DTT (at a thiol/ene ratio of 0.9), and photoinitiator LAP (1 mM). Gelation was initiated by 365 nm light (5 mW/cm^2) for 2 min. Resulting gels were transferred to PBS, kept from light, and allowed to swell prior to confocal imaging. For SEM imaging, hydrogels were fabricated and cut in half with a razor blade and affixed to the stub via magnetic tape. The samples were gold coated via a Denton Vacuum Desk V sputter. The surface of the cut gel was imaged using a JOEL JSM-7800f Field

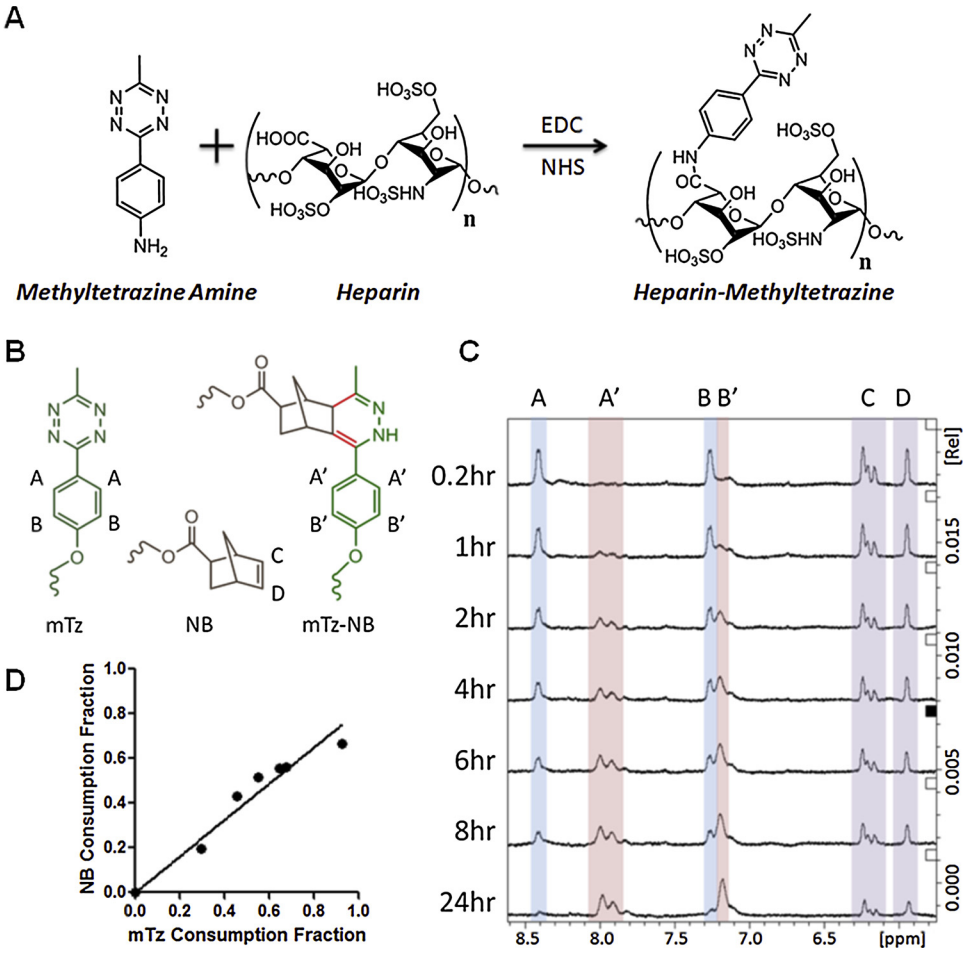

Fig. 3. (A) Synthesis of mTz-Hep. (B) Reaction between mTz-Hep and mPEGNB. (C) Overlay of ^{1}H NMR chromatographs of mTz-Hep and mPEGNB. (D) Correlation of mTz and NB consumptions.

Table 3
DLS measurements of DS coated layered nanoparticles pre and post ara-C loading (PLL 0.25 mg/mL at the core).

	Ara-C Loading	Zeta Potential (mV)	Size (nm)	PDI
DS-coated NPs	Pre	−48.5 ± 0.7	127.0 ± 2.5	0.143 ± 0.002
	Post	−43.4 ± 2.5	109.8 ± 2.9	0.113 ± 0.022
Hep-coated NPs	Pre	−45.2 ± 4.1	127.2 ± 2.5	0.142 ± 0.001
	Post	−32.2 ± 5.1	106.8 ± 2.0	0.109 ± 0.015

Emission SEM.

Lysozyme was used as a model protein for assessing enhanced protein loading in NP-laden hydrogels. Layered NPs with heparin on the surface were prepared as described above and loaded in hydrogels at 7.3 wt%. NP-loaded hydrogels were swelled in PBS overnight and washed twice to remove unreacted material, followed by drying in a desiccator. Next, dried hydrogels were transferred to lysozyme solution (0.25 μg/mL) and placed on a shaker in a 4 °C refrigerator. Samples aliquots were collected and stored in −80 °C freezer until all materials were ready for protein quantification using a Micro BCA Protein Assay Kit (Thermo Scientific).

2.5. Nanoparticle cytotoxicity and intracellular uptake

Cytotoxicity of PLL, Hep, DS, and 1.3x Hep/PLL NPs with equal concentration of PLL in solution and NPs was tested using J774A.1 cells. Cells were seeded at 5,000 cells per well in a 96 well plate. After reaching near 80 % confluence, cells were treated with the materials for 3 h, followed by MTT assay (0.4 mg/mL thiazolyl blue tetrazolium bromide dissolved in serum free DMEM high glucose). After 2 h of MTT incubation, precipitates were dissolved by adding DMSO MTT absorbance at 570 nm was obtained with a microplate reader and normalized to negative controls. To assess intracellular uptake of NPs, 75,000 J774A.1 (or 100,000 NIH 3T3 cells) were seeded on a 35 mm tissue culture plate. To activate J774A.1 cells, 1 μg/mL lipopolysaccharide (LPS) was added to the culture 1 day before adding NPs. DS, Hep, or Hep-Tz coated layered NPs were prepared with 0.25 mg/mL of PLL-FAM. Hep-Tz layered NPs were further reacted with methyl-PEGNB at (mPEGNB, 5.5x NB:Tz molar ratio) for 24 h. All NPs were diluted 10-fold with cell culture media (high glucose DMEM supplemented with 10 % fetal bovine serum and 1 % antibiotic-antimycotic) and added to cell culture for four hours. After which, the cells were fixed with 4 % paraformaldehyde, permeabilized with saponin, and counterstained with DAPI. Images were taken with a confocal microscope (Olympus Fluoview FV100 laser scanning microscope) and analyzed by ImageJ.

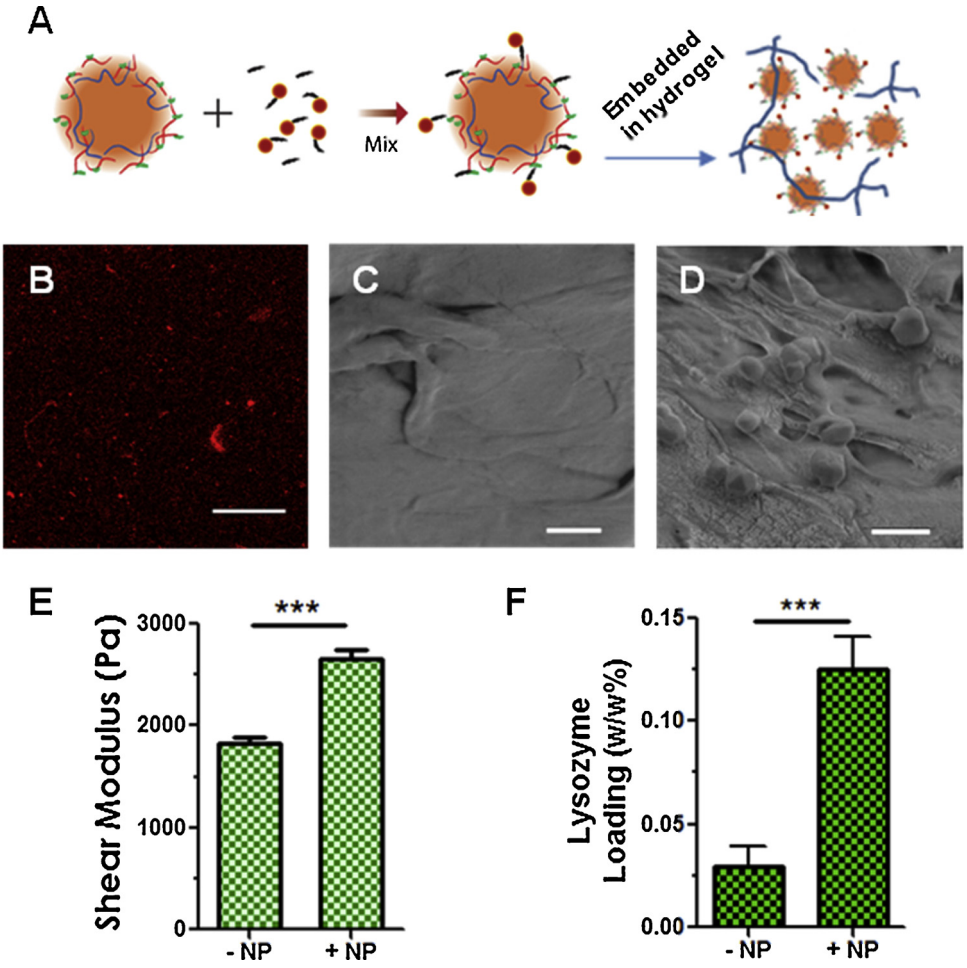

Fig. 4. (A) Schematic of NP PEGylation using Tz-NB click chemistry. (B) Confocal image of Cy5-PEGylated NPs entrapped in a hydrogel (Scale: 200 μm). (C) SEM images of PEG8NB-DTT hydrogel without (C) or with (D) layered NPs (Scales: 1 μm). (E) Shear Modulus on PEG8NB-DTT hydrogels with or without NPs. (F) Lysozyme loading of PEG8NB-DTT hydrogels with or without NPs.

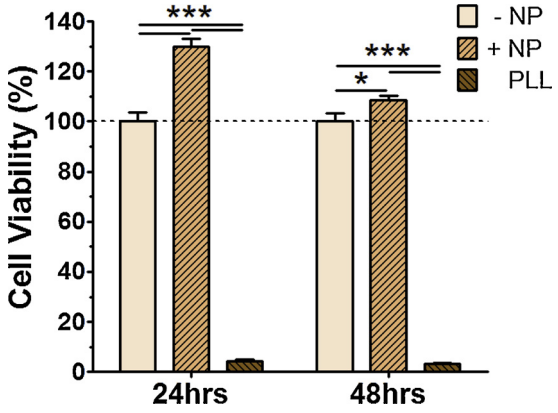

Fig. 5. Effect of Hep/PLL NPs and soluble PLL on J774A.1 cell viability. Soluble PLL at 0.25 mg/mL was used as negative control.

2.6. Ara-C loading to NPs & cell studies

Cytosine-beta-D-arabinofuranose hydrochloride (ara-C) was loaded to NP surface through ionic complexation. Briefly, to a solution of Hep and DS-coated NPs, ara-C was added at a ratio of ten ara-C to one heparin or DS subunit. The resulting solution was stirred at 75 °C for 1 h, centrifuged at 14,000 rpm (4 °C) for 25 min to remove excess ara-C, whose concentration was measured spectrophotometrically (272 nm) and used to determine the drug loading by mass balance calculation. To assess cell killing ability of ara-C loaded NPs, J774A.1 (25,000 cells per well) and MOLM-14 cells (200,000 cells per well) were seeded into a 48 well plate and treated with NP, ara-C, and ara-C loaded NPs. Cells were incubated for 44 h followed by MTT assay as described above.

2.7. Statistical analysis

Quantitative results are reported as mean ± SEM. Two-tailed t-tests and two-way analysis of variance ANOVA with a Bonferroni post-test were utilized in determining of significance. Significance was considered with a p values < 0.05, < 0.01, and < 0.001, corresponding to single, double, and triple asterisks respectively. Experiments were performed in an independent fashion, at least in duplicate.

3. Results & discussion

3.1. Polysaccharide nanoparticle synthesis and characterization

To fabricate polysaccharide nanoparticles (NPs), we first mixed Hep, a polyanion, and PLL, a polycation, at various weight ratios, followed by continuous ultrasonication for 5 min (Fig. 1A). NP sizes and surface charges characterization results showed that the NPs became negatively charged at Hep/PLL weight ratio of 1 or above (Fig. 1B). In addition to using PLL, we tested whether other positively charged polysaccharide (e.g., ChO) could also be used to form NPs with the same method. When ChO was used, the minimum polyanion-polycation ratio needed to generate negatively charged NPs was about 0.75x

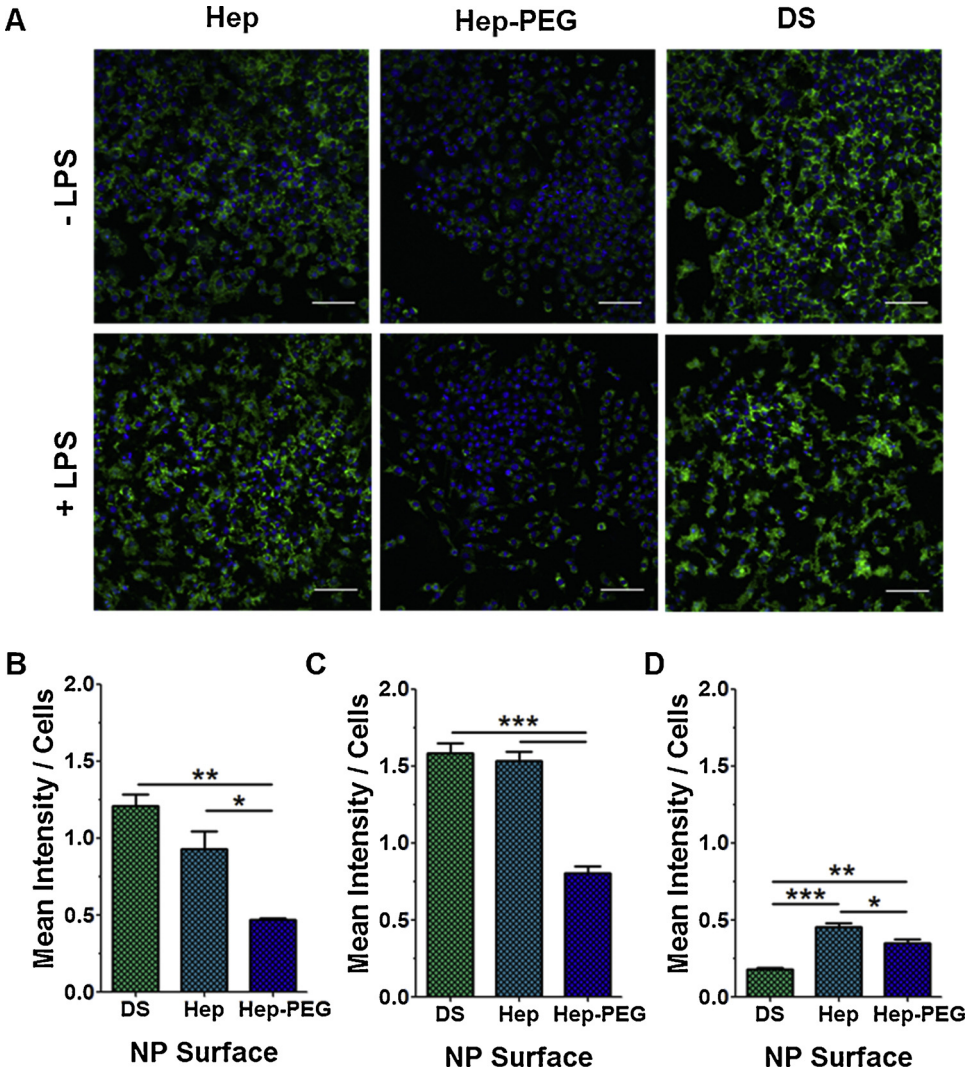

Fig. 6. (A) NP uptake by J77A.1 cells (Green: PLL-FAM. Blue: DAPI. Scales: 100 μm). (B–D) Fluorescent intensity of FAM per cell (~500 cells per image): (B) Non-activated J774A.1 cells. (C) LPS activated J774A.1 cells, and (D) NIH/3T3 cells. (For interpretation of the references to colour in this figure legend, the reader is referred to the web version of this article).

(Fig. 1C). We characterized the sizes of Hep/PLL NPs and found that they had narrow size distribution (averaged to ~120 nm, except at the lowest Hep content) and PDI (~0.17–0.22) regardless of surface charge (Fig. 1D, Table 1A). Replacing PLL with ChO significantly increased the sizes of the NPs from ~120 nm to ~260 nm (Table 1B), potentially due to the bulky D-glucosamine backbone structure of ChO. PLL was used as the core polymer in the remaining studies since it afforded NPs with smaller sizes.

The NPs were highly stable, as demonstrated by the largely overlapping size distribution on day 0 to day 29 post-synthesis (Fig. 1E). In addition to DLS data, we adapted DMMB assay, a method for quantifying glycosaminoglycan content (e.g., heparin), to evaluate the stability of the polysaccharide nanoparticles. Initial measurements of the NPs with 0.7x [Hep]/[PLL] showed undetectable heparin (data not shown), suggesting that DMMB was not able to diffuse into the core of the polysaccharide NP. As such, DMMB assay offers another method for measuring the stability of the NPs, since any degradation/disintegration of NPs would result in liberation of heparin into the solution. Over the course of a month, there was no measurable heparin in the solution incubated with the 0.7x NP (data not shown), suggesting the NP did not disintegrate for at least a month. DMMB results were in agreement with the DLS measurements.

3.2. Pulse sonication for layered nanoparticle fabrication

One of the benefits of using electrostatic interactions for biofabrication is that multiple species with different charges can be layered sequentially to form a layered structure. This approach also affords modular assembly of multiple functional motifs to the surface of NPs. To this end, we have developed a sequential pulse sonication protocol to facilitate layered NP fabrication. Fig. 2A illustrates the steps of the continuous/undisrupted ultrasonication (method i) and a pulse ultrasonication procedure (method ii) to form the central NPs, as well as the procedure to form layered NPs (method iii). The two 'pulse ultrasonication' methods composed of alternating sonication and cool down steps. With continuous ultrasonication (method i), we obtained negatively charged NPs with relatively high PDI (~0.22, Fig. 2B) and an averaged size of ~160 nm (Fig. 2C). Note that in this NP fabrication where Hep/PLL weight ratio was kept at 1.3x, higher concentrations of Hep (2.0 mg/mL) and PLL (1.54 mg/mL) were used in order to scale up NP fabrication. As a result, both NP size and PDI were significantly increased from the previous study where lower Hep and PLL concentrations were used (0.325 mg/mL and 0.25 mg/mL, respectively). We reasoned that increasing ultrasonication time would reduce size and PDI of the NPs. However, continuous ultrasonication passing 5 min caused the vessel to heat up drastically even with the use of an ice bath.

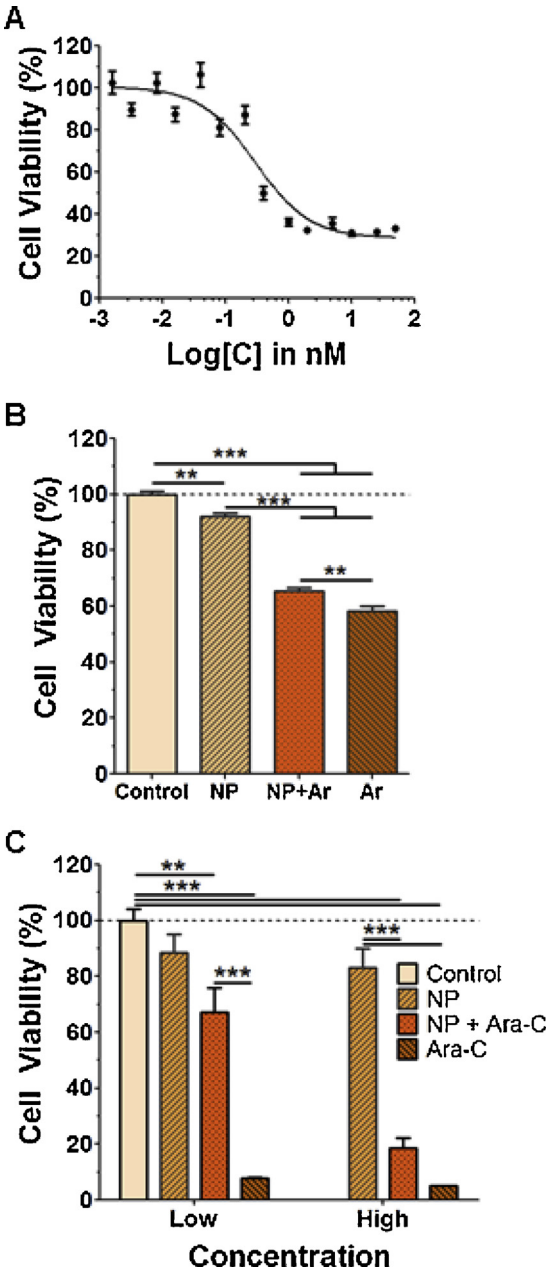

Fig. 7. (A) Effect of [ara-C] on Molm14 viability. (B) Molm14 viability under different NP treatments. Ara-C: 0.3 nM. (C) J774A.1 viability with NP (Low: 0.021 mg/mL; High: 0.102 mg/mL), soluble Ara-C (Low: 9.2 nM; High: 46 nM), and Ara-C loaded NPs with equivalent concentrations.

Therefore, we added additional 'cool down' steps in between ultrasonication steps (method ii, Fig. 2A). As shown in Fig. 2B and C, pulse ultrasonication method yielded NPs with significantly lower size and PDI, two indices critical for endocytosis, drug loading efficiency and release rate.

Method ii was further modified for forming layered NPs consisted of a core NP with 0.7x [Hep]/[PLL]. Upon the addition of heparin mid-cooling (method iii, Fig. 2A), the overall [Hep]/[PLL] became 1.3x (i.e., negatively charged). DLS characterization results showed that layered NPs were formed with a small PDI (Fig. 2B), a slightly larger size (Fig. 2C), and an overall negative surface potential (Fig. 2D). It is worth noting that NPs formed at 0.7x [Hep]/[PLL] initially exhibited a positive surface potential (Fig. 1B). After layering additional Hep, the surface charge changed to negative with accompanying increase in NP size, suggesting that the additional material was successfully layered to the surface of the NPs. This fabrication method was used to form dextran sulfate (DS) shell NPs. The size, zeta potential, and PDI were similar between that in Hep shell NPs (Hep and DS groups, Table 2). The pulse ultrasonication method developed here provides an easy means of constructing modular NPs with the same core NPs but different surface polysaccharides.

3.3. Decorating layered NPs with clickable handles

To afford 'clickable' modification of layered NP surface (e.g., PEGylation, antibody conjugation, etc.), (methyl)tetrazine-modified heparin (i.e., Hep-(m)Tz) was used. (m)Tz group was selected as it readily react with norbornene (NB)-functionalized molecules through Tz-NB click chemistry. Tz-Hep and mTz-Hep were first synthesized via standard carbodiimide chemistry using Tz-amine or mTz-amine (Fig. 3A). The reactivity of Hep-mTz with NB moiety (in the form of a linear methyl-PEG-NB, Fig. 3B) was monitored by ^{1}H NMR (Fig. 3C). Reactions between mTz and NB moieties resulted in shifting of proton peaks corresponding to the hydrogen atoms of the mTz aromatic ring (peaks A, A', B, B') and reduction of NB associated protons (peaks C and D). Fig. 3D shows the correlation of mTz and NB consumption, which yielded linear and quantitative reaction kinetics (R^2 = 0.944). Note that there was residual NB proton signals left after 24 h of reaction. This could be attributed to the amount of mTz and NB added were both based on best effort estimation, resulting in excess NB than mTz motifs in the starting reaction mixture. The error in the functional group estimation could also be attributed to the heterogeneous nature of heparin. Regardless, the reaction proceeded spontaneously and was completed by 24 h. Furthermore, mTz-Hep was used successfully to form layered NPs through the pulse ultrasonication protocol (Fig. 2A. Method iii). Compared with using Hep, both Hep-Tz and Hep-mTz layered NPs still exhibited negatively charged surface but with slightly larger sizes (likely due to the added Tz/mTz groups) and narrower PDIs (Hep-Tz, Hep-mTz groups, Table 3). The installation of clickable handles on the surface of nanoparticles facilitates modular modification of inert (e.g., PEG) or functional/bioactive motifs (e.g., peptides, antibodies, etc.) for desired biomedical applications.

3.4. Click-modification of NP surface and hybrid NP-laden hydrogels

After demonstrating Hep-Tz and Hep-mTz could be used to effectively form layered NPs via pulse ultrasonication, we next sought to explore the surface-tethered Tz/mTz motifs as clickable handles for bioconjugation (e.g., PEGylation). To this end, a linear Cy5-PEG-NB was synthesized and employed for easy monitoring of PEGylation through simple mixing of Hep-Tz coated NPs with Cy5-PEG-NB (Fig. 4A). Hep-Tz covered NPs were mixed with Cy5-PEG-NB and incubated for 24 h. After removing unreacted Cy5-PEG-NB, the Cy5-tagged, PEGylated NPs were further entrapped into a thiol-norbornene hydrogel for visualization via confocal microscopy (Fig. 4A). The dotty red Cy5 fluorescence in the images was indicative of successful tagging of Cy5, and hence PEGylation, on the surface of the polysaccharide layered NPs. Aggregation was noted and the origin was determined to be from the centrifugation steps, since repeated studies without concentration step showed no aggregation (data not shown). Collectively, these results have demonstrated that the NB-PEG-Cy5 species were successfully 'clicked' onto the NP surface and demonstrated that the Tz motif on the NP surface and were available to react with other norbornene modified species. Owing to the modular reactivity of Tz-NB click reaction, it is possible to click different bioactive motifs simultaneously or sequentially to increase the functionality of the clickable NPs.

To demonstrate that polysaccharide NPs can act as a reservoir for protein sequestration, we incorporated Hep-Tz NPs into thiol-norbornene hydrogels crosslinked by 3 wt% PEG8NB and DTT with a thiol/ene ratio of 0.9. NP-free and NP-laden hydrogels were imaged by SEM

(Fig. 4C and D, respectively), which showed clear NP presence only in the NP-laden hydrogels. Rheometry measurement of gel stiffness revealed a significant increase in shear modulus (G') when NPs are incorporated into the hydrogel (Fig. 4E), which might be due to the additional Tz-NB click reaction contributing to crosslinking density. Finally, lysozyme uptake results showed a significant increase in protein loading in hydrogels with the incorporation of Hep-Tz NPs (Fig. 4F), suggesting that this material system may be beneficial for affinity based sequestration and release of therapeutic proteins.

3.5. Cytocompatibility of clickable layered nanoparticles

Cytocompatibility of polysaccharide NPs and their constituent polymers were evaluated via MTT assays on J774A.1 monocytes. Not surprisingly, addition of soluble PLL at the NP forming concentration (i.e., 0.25 mg/mL) almost led to complete cell death after 24 h of culture (Fig. 5). Addition of soluble heparin at the NP forming concentration did not exert any adverse effect of cell growth (data not shown). Interestingly, layered NPs (with same PLL concentration at the NP core) added to the cell culture increased J774A.1 cell proliferation. In spite of the use of a soluble PLL concentration that would have cause cell death, NPs formed at this PLL concentration actually promoted cell proliferation as more than 100 % of MTT signals were obtained from these samples when compared with the control group. It was possible that these NPs, which were 'heparinized' on the surface, sequestered more serum proteins and resulted in increased uptake by the cells. Consequently, forming NPs with surface heparin exerted an unexpected effect on promoting cell proliferation. When dextran sulfate was used as the shell of the NPs, no cytotoxic effect was observed (data not shown).

3.6. Intracellular uptake of modular layered nanoparticles

Modulation of cellular uptake/recognition of NP is of upmost importance for targeted delivery of therapeutics to cells. When delivered into the body, NPs can be cleared by macrophages, which is problematic for therapeutic applications of nanoparticle. Strategies to increase NP circulation time are therefore important as they can increase the amount of drug getting to the desired location. Modulating uptake/recognition could also increase interaction of a nanoparticles with a specific cell type for the treatment. As such, we attempted to modulate the uptake of our clickable layered NPs using monocyte/macrophage cell line J774A.1. Building from the same 'core' NP (i.e., 0.7x [Hep]/[PLL]), we fabricated NPs with heparin, Hep-Tz, or dextran sulfate (DS) at the surface. Hep-Tz was used as it endowed the NPs with a click chemistry handle for facile PEGylation (through reacting with linear PEGNB), which 'shields' the NPs from macrophages, thereby increasing circulation time (Fig. 4A). On the other hand, DS was used because of its macrophage targeting capability (Heo et al., 2017; Kim et al., 2013).

The studies were performed on naïve (non-LPS treated) and LPS-activated J774A.1 cells since monocytes (e.g., naïve J774A.1) and macrophages (e.g., LPS-activated J774A.1) are both immune cells that are likely to come in contact with NPs. A non-immune cell type, NIH/3T3 fibroblast was used as a non-target cell control. To visualize NP uptake by the cells, PLL was first fluorescently labeled with 5(6)-carboxyfluorescein (i.e., PLL-FAM) prior to incorporating into the NPs. Since macrophages are in tissue, this cell type is likely to come in contact with NPs, potentially close to the site of treatment. As such, the NPs were administered to LPS activated J774A.1 macrophages, which exhibited an M1 phenotype (Bartosh, Ylostalo, Bazhanov, Kuhlman, & Prockop, 2013; Bartosh & Ylostalo, 2014; Murray & Wynn, 2011). Regardless of LPS treatment, however, there was a clear decrease of 5(6)-FAM fluorescence in the PEGylated-NPs treated cells (Fig. 6A), whereas DS-NPs were taken up effectively by the cells. Note that these PEGylated NPs still contained heparin on the surface but the PEG 'clicked' to the NP surface effectively reduced intracellular uptake. LPS treatment activated J774A.1 cells, as demonstrated by higher degree of cell spreading (Fig. 6A). The morphology of the cells treated with PEGylated NPs were more circular, suggesting that the cells remained as naïve monocytes. However, there was more spreading in the cells treated with either DS or heparin-coated nanoparticles, suggesting that the cells could have been activated due to the uptake of NPs (Fig. 6A). To quantify cellular uptake of different NPs, fluorescent intensity was normalized to cell number (Fig. 6B, C). When comparing cellular uptake results, two phenomena are worth noting. First, the levels of NP uptake by LPS-activated J774A.1 cells were higher than that in non-activated cells. Second, PEGylation of NPs significantly decreased cellular uptake, which is in agreement with previous literature (Bamberger, Hobernik, Konhauser, Bros, & Wich, 2017; Kaul & Amiji, 2002; Peracchia et al., 1999; Sanchez, Yi, & Yu, 2017; Viard et al., 2018). Furthermore, comparing NPs coated with Hep-Tz and with heparin, there was no significant difference in the amount of NP uptake by the cells (data not shown). Therefore, it can be concluded that the surface tetrazine was not responsible for the decrease in cellular uptake for the PEGylated group. Furthermore, J774A.1 cells clearly uptake more NPs than 3T3 fibroblasts, regardless of NP formulations (Fig. 6D). Within the fibroblasts study, there was a small increase in uptake of Hep-NPs than DS-NPs, potentially due to increase in serum protein complexation that improved their intracellular uptake. Fig. 6 shows that DS-NPs can be employed to aid in macrophage targeting, a result consistent with literature reports (Heo et al., 2017; Platt, Suzuki, Kurihara, Kodama, & Gordon, 1996).

3.7. Drug loading and delivery via NP-complexation

Off targeting toxicity is a major problem for therapeutic administration, so employing a nanoparticle carrier could be beneficial for minimizing off-target cytotoxicity while maximizing the intended therapeutic efficacy. To demonstrate the therapeutic delivering potential of our polysaccharide layered nanoparticles, cytosine-beta-D-arabinofuranose hydrochloride (also known as cytarabine or ara-C, a standard chemotherapeutic used to treat multiple forms of leukemia) was loaded to NPs and exposed to an acute leukemia cell line (Molm-14) and J774A.1 cells. Loading of ara-C to Hep-NPs or DS-NPs was achieved via ionic complexation following an established protocol (Liu et al., 2014). The loading efficiency was determined to be 13.6 % and 17.7 % of ara-C for DS-NP and Hep-NP, respectively. Drug loading onto the surface of DS-NPs or Hep-DS reduced the negative charge (Table 3), suggesting that ara-C had formed polyelectrolyte complexes with Hep or DS. Drug-loaded NP size and PDI were also reduced, likely due to increased compaction of NPs via additional electrostatic interactions.

Prior to testing the effect of ara-C-loaded NPs on cell killing, we determined the LD50 of ara-C for Molm-14 cells to be 0.3 nM (Fig. 7A). Hep-NPs were used to load ara-C at LD50, which demonstrated effective cell killing comparable to that of soluble ara-C (Fig. 7B). The reduction of cytotoxicity of ara-C loaded Hep-NP may be due to ara-C not being completely released from the NP upon cell uptake. For targeting macrophages, we used DS-NPs to load ara-C. Soluble ara-C was highly cytotoxic to J774A.1 cells for the two concentrations tested, whereas ara-C-loaded DS-NPs only induced high level of cytotoxicity at high drug concentration (Fig. 7C). While this in vitro cytotoxicity assay could not resemble the therapeutic efficacy of ara-C-loaded NPs in vivo, our current study demonstrated that both Hep-NP and DS-NP can be used to load ara-C, which induced desired cytotoxic effect. Future work will focus on exploring the modular Tz-NB click chemistry to conjugate cell-targeting ligand onto the NP surface, as well as on evaluating the therapeutic potential of this modular polysaccharide nanoparticle system.

4. Conclusion

We have developed innovative 'clickable' nanoparticles with a layered structure. The synthesis of nanoparticle was facilitated by a

pulse ultrasonication methodology and was highly modular, as demonstrated by the use of several polysaccharides to create NPs with modularly tunable surface properties. Furthermore, the installation of a tetrazine motif on nanoparticle surface permitted facile and modular conjugation of norbornene-tagged molecules (either inert or bioactive) to regulate cellular recognition of the functionalized nanoparticles. We showed that modulating nanoparticle surface properties affected their *in vitro* uptake by naïve or activated macrophages. Furthermore, this nanoparticle platform was adapted as a drug carrier based on ionic complexation. Future work will focus on clicking multiple receptor binding ligands on the surface of the nanoparticles, as well as employing this system for drug delivery applications.

Acknowledgement

This project was supported in part by the National Science Foundation (CAREER Award #1452390) and the National Cancer Institute (Award #R01CA227737).

References

Bamberger, D., Hobernik, D., Konhauser, M., Bros, M., & Wich, P. R. (2017). Surface modification of polysaccharide-based nanoparticles with PEG and dextran and the effects on immune cell binding and stimulatory characteristics. *Molecular Pharmaceutics, 14*, 4403–4416.

Bartosh, T. J., & Ylostalo, J. H. (2014). Macrophage inflammatory assay. *Bio Protocol, 4*.

Bartosh, T. J., Ylostalo, J. H., Bazhanov, N., Kuhlman, J., & Prockop, D. J. (2013). Dynamic compaction of human mesenchymal stem/precursor cells into spheres self-activates caspase-dependent IL1 signaling to enhance secretion of modulators of inflammation and immunity (PGE2, TSG6, and STC1). *Stem Cells, 31*, 2443–2456.

Bobo, D., Robinson, K. J., Islam, J., Thurecht, K. J., & Corrie, S. R. (2016). Nanoparticle-based medicines: A review of FDA-Approved materials and clinical trials to date. *Pharmaceutical Research, 33*, 2373–2387.

Chen, C., Li, S., Liu, K., Ma, G., & Yan, X. (2016). Co-assembly of heparin and polypeptide hybrid nanoparticles for biomimetic delivery and anti-thrombus therapy. *Small, 12*, 4719–4725.

Danaei, M., Dehghankhold, M., Ataei, S., Hasanzadeh Davarani, F., Javanmard, R., Dokhani, A., ... Mozafari, M. R. (2018). Impact of particle size and polydispersity index on the clinical applications of lipidic nanocarrier systems. *Pharmaceutics, 10*.

Dumitrescu, L., Constantinescu, C. S., & Tanasescu, R. (2018). Recent developments in interferon-based therapies for multiple sclerosis. *Expert Opinion on Biological Therapy, 18*, 665–680.

Fairbanks, B. D., Schwartz, M. P., Bowman, C. N., & Anseth, K. S. (2009). Photoinitiated polymerization of PEG-diacrylate with lithium phenyl-2,4,6-trimethylbenzoylphosphinate: Polymerization rate and cytocompatibility. *Biomaterials, 30*, 6702–6707.

Fairbanks, B. D., Schwartz, M. P., Halevi, A. E., Nuttelman, C. R., Bowman, C. N., & Anseth, K. S. (2009). A versatile synthetic extracellular matrix mimic via Thiol-Norbornene Photopolymerization. *Advanced Materials, 21*, 5005–5010.

Farndale, R. W., Buttle, D. J., & Barrett, A. J. (1986). Improved quantitation and discrimination of sulphated glycosaminoglycans by use of dimethylmethylene blue. *Biochimica et Biophysica Acta, 883*, 173–177.

Han, H. S., Devaraj, N. K., Lee, J., Hilderbrand, S. A., Weissleder, R., & Bawendi, M. G. (2010). Development of a bioorthogonal and highly efficient conjugation method for quantum dots using tetrazine-norbornene cycloaddition. *Journal of the American Chemical Society, 132*, 7838–7839.

Heo, R., You, D. G., Um, W., Choi, K. Y., Jeon, S., Park, J. S., Choi, Y., Kwon, S., Kim, K., Kwon, I. C., Jo, D. G., Kang, Y. M., & Park, J. H. (2017). Dextran sulfate nanoparticles as a theranostic nanomedicine for rheumatoid arthritis. *Biomaterials, 131*, 15–26.

Huckaby, J. T., & Lai, S. K. (2018). PEGylation for enhancing nanoparticle diffusion in mucus. *Advanced Drug Delivery Reviews, 124*, 125–139.

Kaul, G., & Amiji, M. (2002). Long-circulating poly(ethylene glycol)-modified gelatin nanoparticles for intracellular delivery. *Pharmaceutical Research, 19*, 1061–1067.

Kim, S. H., Kim, J. H., You, D. G., Saravanakumar, G., Yoon, H. Y., Choi, K. Y., ... Park, J. H. (2013). Self-assembled dextran sulphate nanoparticles for targeting rheumatoid arthritis. *Chemical Communications (Cambridge, England), 49*, 10349–10351.

Liu, J., Jiang, Y., Cui, Y., Xu, C., Ji, X., & Luan, Y. (2014). Cytarabine-AOT catanionic vesicle-loaded biodegradable thermosensitive hydrogel as an efficient cytarabine delivery system. *International Journal of Pharmaceutics, 473*, 560–571.

Liu, T., Hu, Y., Tan, J., Liu, S., Chen, J., Guo, X., ... Li, X. (2017). Surface biomimetic modification with laminin-loaded heparin/poly-l-lysine nanoparticles for improving the biocompatibility. *Materials Science & Engineering C, Materials for Biological Applications, 71*, 929–936.

Murray, P. J., & Wynn, T. A. (2011). Protective and pathogenic functions of macrophage subsets. *Nature Reviews Immunology, 11*, 723–737.

Okamoto, A., Asai, T., Hirai, Y., Shimizu, K., Koide, H., Minamino, T., et al. (2018). Systemic administration of siRNA with Anti-HB-EGF antibody-modified lipid nanoparticles for the treatment of triple-negative breast cancer. *Molecular Pharmaceutics, 15*, 1495–1504.

Peng, X. H., Wang, Y., Huang, D., Wang, Y., Shin, H. J., Chen, Z., Spewak, M. B., Mao, H., Wang, X., Wang, Y., Chen, Z. G., Nie, S., & Shin, D. M. (2011). Targeted delivery of cisplatin to lung cancer using ScFvEGFR-heparin-cisplatin nanoparticles. *ACS Nano, 5*, 9480–9493.

Peracchia, M. T., Fattal, E., Desmaele, D., Besnard, M., Noel, J. P., Gomis, J. M., ... Couvreur, P. (1999). Stealth PEGylated polycyanoacrylate nanoparticles for intravenous administration and splenic targeting. *Journal of Controlled Release: Official Journal of the Controlled Release Society, 60*, 121–128.

Phua, K. K., Nair, S. K., & Leong, K. W. (2014). Messenger RNA (mRNA) nanoparticle tumour vaccination. *Nanoscale, 6*, 7715–7729.

Platt, N., Suzuki, H., Kurihara, Y., Kodama, T., & Gordon, S. (1996). Role for the class A macrophage scavenger receptor in the phagocytosis of apoptotic thymocytes in vitro. *Proceedings of the National academy of Sciences of the United States of America, 93*, 12456–12460.

Rodriguez, P. L., Harada, T., Christian, D. A., Pantano, D. A., Tsai, R. K., & Discher, D. E. (2013). Minimal "Self" peptides that inhibit phagocytic clearance and enhance delivery of nanoparticles. *Science, 339*, 971–975.

Sanchez, L., Yi, Y., & Yu, Y. (2017). Effect of partial PEGylation on particle uptake by macrophages. *Nanoscale, 9*, 288–297.

Suk, J. S., Xu, Q., Kim, N., Hanes, J., & Ensign, L. M. (2016). PEGylation as a strategy for improving nanoparticle-based drug and gene delivery. *Advanced Drug Delivery Reviews, 99*, 28–51.

Tian, F., Dahmani, F. Z., Qiao, J., Ni, J., Xiong, H., Liu, T., ... Yao, J. (2018). A targeted nanoplatform co-delivering chemotherapeutic and antiangiogenic drugs as a tool to reverse multidrug resistance in breast cancer. *Acta Biomaterialia, 75*, 398–412.

Tran, S., DeGiovanni, P. J., Piel, B., & Rai, P. (2017). Cancer nanomedicine: A review of recent success in drug delivery. *Clinical and Translational Medicine, 6*, 44.

Viard, M., Reichard, H., Shapiro, B. A., Durrani, F. A., Marko, A. J., Watson, R. M., Pandey, R. K., & Puri, A. (2018). Design and biological activity of novel stealth polymeric lipid nanoparticles for enhanced delivery of hydrophobic photodynamic therapy drugs. *Nanomedicine, 14*, 2295–2305.

Zhang, Y., Lin, L., Liu, L., Liu, F., Maruyama, A., Tian, H., et al. (2018). Ionic-crosslinked polysaccharide/PEI/DNA nanoparticles for stabilized gene delivery. *Carbohydrate Polymers, 201*, 246–256.